

# MODELING AND SIMULATING OF SINGLE SIDE SHORT STATOR LINEAR INDUCTION MOTOR WITH THE END EFFECT

Hamed HAMZEHBAHMANI \*

Linear induction motors are under development for a variety of demanding applications including high speed ground transportation and specific industrial applications. These applications require machines that can produce large forces, operate at high speeds, and can be controlled precisely to meet performance requirements. The design and implementation of these systems require fast and accurate techniques for performing system simulation and control system design. In this paper, a mathematical model for a single side short stator linear induction motor with a consideration of the end effects is presented; and to study the dynamic performance of this linear motor, MATLAB/SIMULINK based simulations are carried out, and finally, the experimental results are compared to simulation results.

**Key words:** linear induction motor (LIM), magnetic flux distribution, dynamic model, end effect, propulsion force

## 1 INTRODUCTION

The linear induction motor (LIM) is very useful at places requiring linear motion since it produces thrust directly and has a simple structure, easy maintenance, high acceleration/deceleration and low cost. Therefore nowadays, the linear induction motor is widely used in a variety of applications such as transportation, conveyor systems, actuators, material handling, pumping of liquid metal, sliding door closers, curtain pullers, robot base movers, office automation, drop towers, elevators, *etc.* In a linear induction motor, the primary winding corresponds to the stator winding of a rotary induction motor (RIM), while the secondary corresponds to the rotor. Normally, the secondary, similar to the RIM rotor, often consists of a sheet conductor, such as copper or aluminum, with a solid back iron acting as the return path for the magnetic flux. Based on the relative primary and secondary length, linear induction motors are categorized into two types: long rotor and short rotor. The structures of these LIMs are shown in Figs. 1a and 1b, respectively [1–3]. The photograph of the experimental model of short stator LIM, constructed for this research is shown in Fig. 2. Table 1 shows its specifications.

The LIM special structure means that its performance is a little different from that of a RIM. As we know, in the RIM, an accurate equivalent circuit model can be derived easily by simplifying the geometry per pole. The main difference between LIM and RIM is related to the “End Effects” which is explained in part 3. These effects should be considered in both the modelling and controlling of LIMs.

In recent decades, a number of papers on the LIM performance analysis, involving steady and dynamic states, have been available [1–15]. Gieras *et al* [4] and Faiz *et*

*al* [5] developed an equivalent circuit by superposing the synchronous wave and the pulsating wave caused by the end effect. Nondahl *et al* [6] derived an equivalent circuit model from the pole-by-pole method based on the winding functions of the primary windings.

**Table 1.** Experimental model specifications

Quantity	Unit	Value
Primary length	Cm	27
Primary width	Cm	9.5
Length of secondary sheet	m	6
Thickness of Secondary Sheet	mm	5
Number of Slots	-	7
Width of Slots	mm	13
High of Slots	mm	37
Air gap length	mm	15
Number of poles	-	2
Number of coils per phase	-	2
Number of turns per coil	-	300
Conductivity of the rotor material	$\Omega^{-1}\text{m}^{-1}$	$2.29 \times 10^7$

Duncan *et al* [7] developed the ‘per-phase’ equivalent circuit by modifying the magnetizing branch of the equivalent circuit of the RIM. Noting that the air gap flux grows and decays gradually from the entry and the exit, respectively, he introduced a weighting function with the use of a dimensionless factor  $Q$ .

Then, the average values were taken to describe the magnetizing inductance and the resistance of the eddy loss. Kang *et al* [8], according to the result in [7], deduced the two-axis models (dq), which can be applied in vector control or direct force control to predict the LIM dynamic performance. However, the derivation process of the revised function  $f(Q)$  is very coarse on the assumption that

\* Islamic Azad University Sanandaj Branch Sanandaj, hamedpwr@yahoo.com

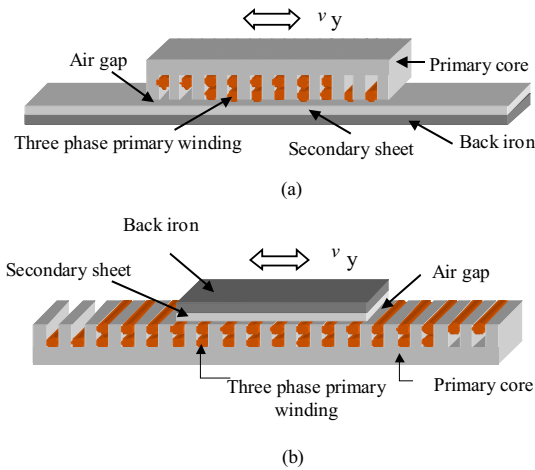


Fig. 1. Linear Induction Motor with (a) Short Stator (b) Short Rotor



Fig. 2. Experimental model of short stator linear induction motor

the eddy current in the secondary sheet decreases from maximum to zero by exponential attenuation only in the primary length range. It only considers the mutual inductance influenced by the eddy current, disregarding its effect on the secondary resistance.

In this paper, in order to investigate the magnetic flux distribution, first a 2-D model of LIM is simulated and the circumstance of the magnetic flux density and the equipotential lines of the magneto static potential in the core and its surrounding for steady cases are presented. Then, based on the per-phase equivalent circuit in [8], a mathematical model for the single side short stator linear induction motor with a consideration of the end effects is presented. In order to verify the mathematical model, a laboratory prototype of short stator LIM is developed and the results of experiments and simulations are presented in Section 7. In this section, first, the equivalent circuit parameters are obtained and compared with calculation results. Then, two experiments, a free acceleration and locked primary experiment ( $S = 1$ ) have been done and the results have been compared with the simulation re-

sults. A comparison of the experiments results with the calculation and simulation results show that the calculation and simulation procedure and the obtained model for this type of linear motor have sufficient accuracy.

## 2 MAGNETIC FLUX DISTRIBUTION FOR STEADY CASES

Distribution of the magnetic flux density in the core and surroundings of the experimental model is investigated in this section. Two fundamental postulates of the magneto static that specify the divergence and the curl of  $B$  in free space are [9]

$$\vec{\nabla} \times \vec{H} = \vec{J}, \tag{1}$$

$$\vec{\nabla} \cdot \vec{B} = 0. \tag{2}$$

By using the equation  $\vec{B} = \mu_0 \vec{H}$ , we obtain from (2):

$$\vec{\nabla} \times \vec{B} = \mu_0 \vec{J}. \tag{3}$$

Where  $B$  is the magnetic flux density,  $H$  is the magnetic field intensity,  $J$  is the current density, and  $\mu$  is the magnetic permeability of material. It follows from (1) that there exists a magnetic vector potential  $\vec{A}$  such that

$$\vec{B} = \vec{\nabla} \times \vec{A}, \tag{4}$$

$$\vec{\nabla} \times \left( \frac{1}{\mu} \vec{\nabla} \times \vec{A} \right) = \vec{J}. \tag{5}$$

For 2-D case, the magnetic flux density  $B$  is calculated as

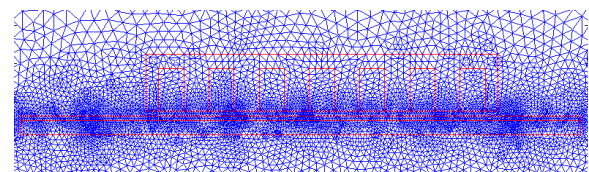
$$\mathbf{B} = \left( \frac{\partial A}{\partial x}, \frac{\partial A}{\partial y}, 0 \right). \tag{6}$$

On the other hand

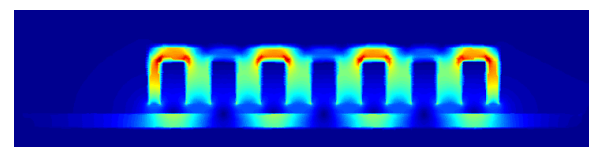
$$\Phi = \int_S \vec{B} \cdot d\vec{s}. \tag{7}$$

From (4) we have:

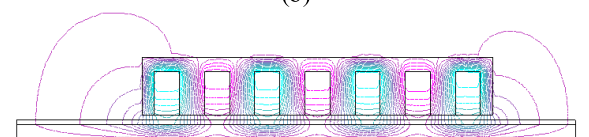
$$\Phi = \int_S (\vec{\nabla} \times \vec{A}) \cdot d\vec{s} = \oint_C \vec{A} \cdot d\vec{l}. \tag{8}$$



(a)



(b)



(c)

Fig. 3. (a) Mesh shape (b) magnetic flux density (c) equipotential lines of the magneto static potential

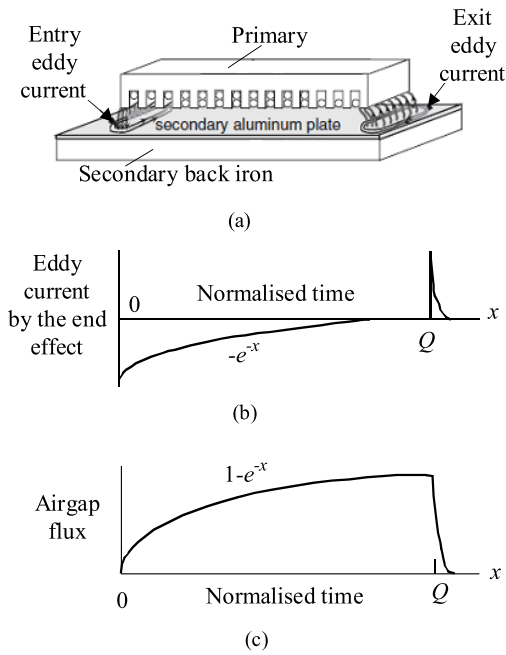


**Fig. 4.** Linear induction motor (a) Eddy-current generation at the entry and exit of the air gap (b) Eddy-current density profile along the length of LIM (c) Air gap flux profile [8]

Using (1) to (8), the magnetic flux density and equipotential lines of the magneto static potential in the core and its surroundings of the experimental model is simulated and the results are shown in Fig. 3. Figure 3a shows the mesh shape of the experimental model and Figs. 3b and 3c show the magnetic flux density and equipotential lines of the magneto static potential, respectively.

### 3 END EFFECT OF LINEAR INDUCTION MOTOR

In LIMs, as the primary moves, a new flux is continuously developed at the entry of the primary yoke, while existing flux disappears at the exit side. Sudden generation and disappearance of the penetrating field causes eddy currents in the secondary plate. This eddy current affects the air gap flux profile in the longitudinal direction. The losses, as well as the flux-profile attenuation, become severer as the speed increases. Such a phenomena is called end effect' of LIM. The end effects are not very noticeable in conventional induction motors. On the other hand, in LIMs, these effects become increasingly relevant with the increase in the relative velocity between the primary and the secondary. Thus, the end effects will be analyzed as a function of the velocity [8] and [10].

Figure 4a shows a view of a LIM. Both generation and decay of the fields cause the eddy current in the secondary sheet. The eddy current in the entry grows very rapidly to mirror the magnetizing current, nullifying the air gap flux at the entry. On the other hand, the eddy current at the exit generates a kind of wake field, dragging the moving motion of the primary core. The density profile of the eddy current along the length of LIM looks like Fig. 4b.

Hence, the resulting magneto motive force (MMF), and thereby air gap flux, looks like Fig. 4c [8].

The  $Q$  factor is associated with the length of the primary, and to a certain degree, quantifies the end effects as a function of the velocity  $v$  as described by equation (9) [11].

$$Q = \frac{DR_y}{(L_m + L_{ly})v}. \quad (9)$$

Where  $D, R_y, L_m, L_{ly}$  and  $v$  are the primary length, secondary resistance, magnetizing inductance, secondary leakage inductance and velocity. Note that the primary's length is inversely dependent on the velocity, *ie*, for a zero velocity the primary's length may be considered infinite, and the end effects may be ignored. As the velocity increases, the primary's length decreases, increasing the end effects, which causes a reduction of the LIM's magnetization current.

This effect may be quantified in terms of the magnetization inductance with the equation [4] and [11]

$$L'_m = L_m(1 - f(Q)) \quad (10)$$

where

$$f(Q) = \frac{1 - e^{-Q}}{Q}. \quad (11)$$

According to (9) to (11), the spatial distribution of the magnetic flux density along the width of the primary depends on the relative speed between primary and secondary. For null speed of the primary, the LIM can be considered as having an infinite primary and in this case the end effects can be neglected.

### 4 MATHEMATICAL MODEL OF SHORT STATOR LIM

In the dynamic analysis of the electrical machines, a mathematical model should be extracted from their equations so that the resulting model can explain the machine's dynamic behavior with a high level of approximation. In this part, the mathematical model of the short stator linear induction motors is given.

#### 4.1 Per Phase Equivalent Circuit of Short Stator LIM

Per phase equivalent circuit of short stator LIM is shown in Fig. 5 [8].

The voltage equations of the per-phase model shown in Fig. 5 are given by [8]

$$\mathbf{v}_{abcx} = R_x \mathbf{i}_{abcx} + P \boldsymbol{\lambda}_{abcx}, \quad (12)$$

$$\mathbf{v}'_{abcy} = R_y \mathbf{i}'_{abcy} + P \boldsymbol{\lambda}'_{abcy}. \quad (13)$$

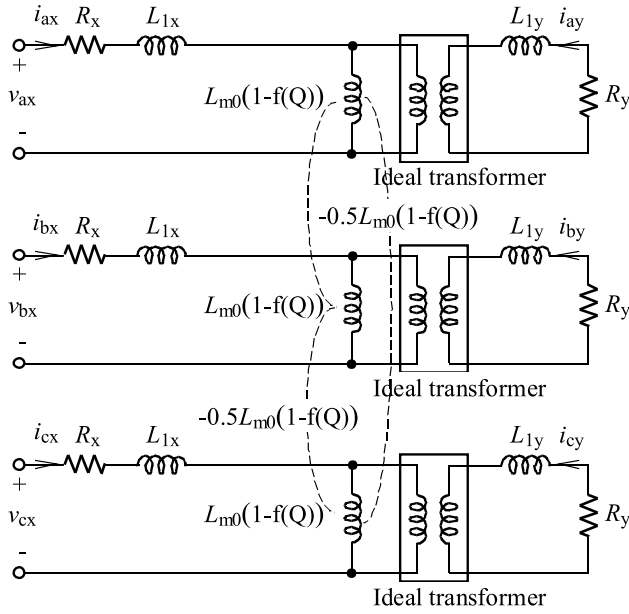


Fig. 5. Per phase equivalent circuit of short stator linear induction motor

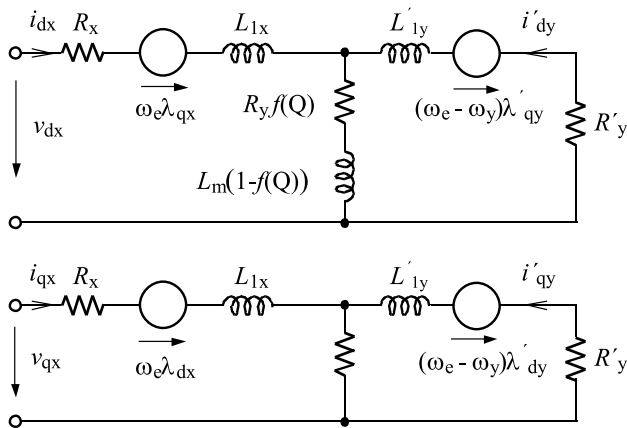


Fig. 6. Equivalent dq circuit of short rotor linear induction motor

Table 2. Equivalent circuit parameters

parameter	Value	
	Experimental result	Computational result
primary resistance $\Omega$ )	12.56	13.22
secondary resistance $\Omega$ )	10.86	9.41
primary leakage inductance (mH)	93.78	97.34
magnetizing inductance (mH)	169.6	188.10

Where  $\mathbf{v}_{abcx} = [v_{ax} \ v_{bx} \ v_{cx}]^T$ ,  $\mathbf{i}_{abcx} = [i_{ax} \ i_{bx} \ i_{cx}]^T$  and  $\boldsymbol{\lambda}_{abcx} = [\lambda_{ax} \ \lambda_{bx} \ \lambda_{cx}]^T$  are the voltage, current and flux linkage of primary, and  $\mathbf{v}'_{abcy} = [v'_{ay} \ v'_{by} \ v'_{cy}]^T$ ,

$\mathbf{i}'_{abcy} = [i'_{ay} \ i'_{by} \ i'_{cy}]^T$  and  $\boldsymbol{\lambda}'_{abcy} = [\lambda'_{ay} \ \lambda'_{by} \ \lambda'_{cy}]^T$  are the voltage, current and flux linkage of the secondary in the secondary frame. Further,  $p$  denotes the differential operator,  $d/dt$ .

To keep the same convention as for the rotary motor, it is assumed that the primary is fixed, while the secondary is moving. The flux-linkage equations for the primary and secondary are given by

$$\boldsymbol{\lambda}_{abcx} = (\mathbf{L}_{lx} + \mathbf{L}_{mx})\mathbf{i}_{abcx} + \mathbf{L}_{my}\mathbf{i}'_{abcy}, \quad (14)$$

$$\boldsymbol{\lambda}'_{abcy} = (\mathbf{L}_{ly} + \mathbf{L}_{mx})\mathbf{i}'_{abcy} + \mathbf{L}_{my}^T\mathbf{i}_{abcx}, \quad (15)$$

where

$$\mathbf{L}_{lx} = \begin{bmatrix} L_{lx} & 0 & 0 \\ 0 & L_{lx} & 0 \\ 0 & 0 & L_{lx} \end{bmatrix}, \quad (16)$$

$$\mathbf{L}_{ly} = \begin{bmatrix} L_{ly} & 0 & 0 \\ 0 & L_{ly} & 0 \\ 0 & 0 & L_{ly} \end{bmatrix}, \quad (17)$$

$$\mathbf{L}_{mx} = L_{m0}(1-f(Q)) \begin{bmatrix} 1 & -\frac{1}{2} & -\frac{1}{2} \\ -\frac{1}{2} & 1 & -\frac{1}{2} \\ -\frac{1}{2} & -\frac{1}{2} & 1 \end{bmatrix}, \quad (18)$$

$$\mathbf{L}_{my} = L_{m0}(1-f(Q)) \times \begin{bmatrix} \cos \theta_y & \cos(\theta_y + \frac{2\pi}{3}) & \cos(\theta_y - \frac{2\pi}{3}) \\ \cos(\theta_y - \frac{2\pi}{3}) & \cos \theta_y & \cos(\theta_y + \frac{2\pi}{3}) \\ \cos(\theta_y + \frac{2\pi}{3}) & \cos(\theta_y - \frac{2\pi}{3}) & \cos \theta_y \end{bmatrix}. \quad (19)$$

$L_{lx}(l_{yx})$  denotes the primary (secondary) leakage and  $\theta_y$  is the angular displacement of the secondary.

#### 4.2 Short stator LIM model in synchronous reference frame

Co-ordinates are changed into a synchronous reference frame with the following transformation map [12]

$$\mathbf{f}_{qd0} = [T_{qd0}(\theta)] \mathbf{f}_{abc}, \quad (20)$$

$$[T_{qd0}(\theta)] = \frac{2}{3} \begin{bmatrix} \cos \theta & \cos(\theta - \frac{2\pi}{3}) & \cos(\theta + \frac{2\pi}{3}) \\ \sin \theta & \sin(\theta - \frac{2\pi}{3}) & \sin(\theta + \frac{2\pi}{3}) \\ \frac{1}{2} & \frac{1}{2} & \frac{1}{2} \end{bmatrix}. \quad (21)$$

Where  $\omega_e$  is the electrical angular velocity and  $f$  is  $v$ ,  $i$  or  $\lambda$ . Utilizing the transformation map (20), we obtain from (12) and (13) the following

$$v_{qx} = R_x i_{qx} + \omega_e \lambda_{dx} + P \lambda_{qx}, \quad (22)$$

$$v_{dx} = R_x i_{dx} - \omega_e \lambda_{qx} + P \lambda_{dx}, \quad (23)$$

$$v'_{qy} = R'_y i'_{qy} + (\omega_e - \omega_y) \lambda'_{dy} + P \lambda'_{qy}, \quad (24)$$

$$v'_{dy} = R'_y i'_{dy} - (\omega_e - \omega_y) \lambda'_{qy} + P \lambda'_{dy}, \quad (25)$$

where  $(v_{qx}, v_{dx})$ ,  $(i_{qx}, i_{dx})$  and  $(\lambda_{qx}, \lambda_{dx})$  are the  $dq$ -axis voltages, currents and flux linkages of the primary,

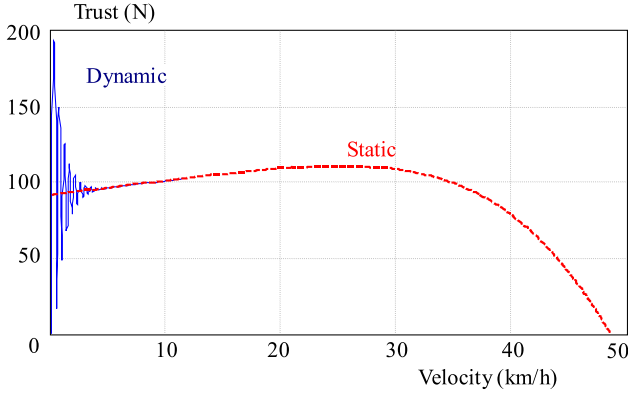


Fig. 7. Dynamic and static thrust-speed simulated characteristic



Fig. 8. Experimental model of LIM under locked test

Table 3. Measured values from free accelerating

Measured value	Unit	Simulation result	Experimental result
Stator voltage	V	380	380
Stator current	A	5.72	5.17
Phase shift	Degree	49.45	52.56

and  $(v'_{qy}, v'_{dy})$ ,  $(i'_{qy}, i'_{dy})$  and  $(\lambda'_{qy}, \lambda'_{dy})$  are the  $dq$ -axis voltages, currents and fluxes of the secondary in the secondary frame, respectively.  $\omega_y$  denotes the secondary angular speed.

Equations (24) and (25) are obtained by the  $|T_{qd0}(\theta \ \theta_y)|$  transformation matrix.

#### 4.3 Flux linkages of the primary and secondary

The  $dq$ -axis flux linkages of the primary and secondary are given by

$$\lambda_{qx} = L_{lx}i_{qx} + L_m(i_{qx} + i'_{qy}), \quad (26)$$

$$\lambda_{dx} = L_{lx}i_{dx} + L_m(1 - f(Q))(i_{dx} + i'_{dy}), \quad (27)$$

$$\lambda'_{qy} = L'_{ly}i'_{qy} + L_m(i_{qx} + i'_{qy}), \quad (28)$$

$$\lambda'_{dy} = L'_{ly}i'_{dy} + L_m(1 - f(Q))(i_{dx} + i'_{dy}). \quad (29)$$

Where  $L_m = 1.5L_{m0}$ .

## 5 EQUIVALENT QD CIRCUIT OF SHORT STATOR LIM

Based on equations (22) to (25), equivalent  $qd$  circuit for short stator LIM obtained as shown in Fig. 6.

## 6 THRUST FORCE

In rotary motors, the machine output is explained as electromagnetic torque in N.m and rotation speed in Rad/sec. On the other hand, in linear motors the machine output is explained as electromagnetic thrust in N and linear speed in m/Sec (or Km/h). Electromagnetic thrust of short stator LIM is given by [8]

$$F_m = \frac{3}{2} \frac{\pi}{\tau_p} [\lambda_{dx}i_{qx} - \lambda_{qx}i_{dx}]. \quad (30)$$

where  $\tau$  is pole pitch of the stator.

## 7 SIMULATION AND EXPERIMENT RESULTS

The dynamic performance of the experimental model is simulated by MATLAB/SIMULINK software. Two different experiments are performed to investigate the validity of the mathematical model. The first is to measure the voltage, current, and the phase shift between them under free acceleration, and the other is an investigation of the air gap effect on the propulsion force under locked primary ( $S = 1$ ).

### 7.1 Measurement of the equivalent circuit parameters

In order to measure the motor parameters, the measurement methods of rotary induction motors and transformers have been used as follows [13]

- DC test for measuring primary resistance ( $R_x$ ).
- Locked secondary test for measuring primary leakage inductance ( $L_x$ ) and secondary resistance ( $R_y$ ).
- Free acceleration test for measuring magnetizing inductance ( $L_m$ ).

On the other hand, the calculation of LIM's parameter has been done according to the method mentioned in [14]. The experimental and computational results of equivalent circuit parameters are shown in Table 2.

Due to the limited length of the machine, it is not possible to achieve the steady state condition in the free acceleration test. Therefore, the maximum error between the two methods on the measurement of the equivalent circuit parameter is about 13%. Nonetheless, this table shows that the accuracy of the method used to measure and calculate the motor parameter is acceptable.

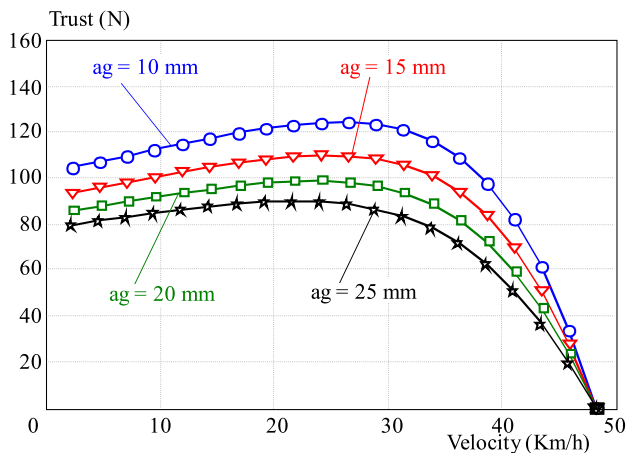


Fig. 9. Tthrust-speed characteristic changing in air gap

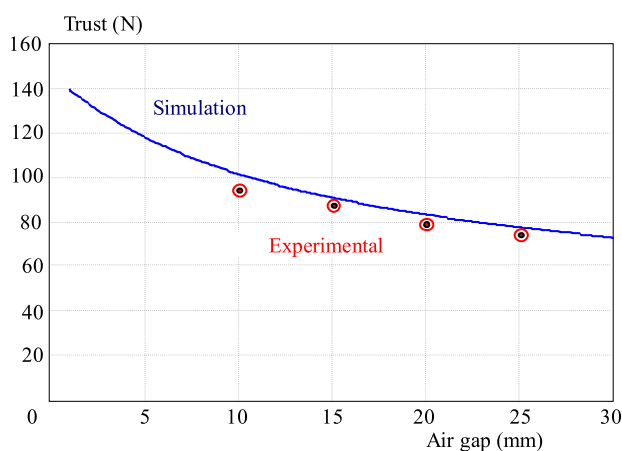


Fig. 10. Propulsion thrust versus air gape length characteristic at unity slip

Table 4. Experiment and simulation result from locked secondary test

Air gape length (mm)	Propulsion force (N)	
	Simulation result	Experimental result
10	102.2	95
15	91.5	88
20	83.8	80
25	78.2	75

7.2 Free acceleration experiment

The thrust versus speed simulated characteristic of the experimental model during free acceleration is shown in Fig. 7. The synchronous speed of this LIM in 50 Hz frequency is 48.54 km/h.

As has been mentioned in part 7.1, due to the limited length of the machine, it is not possible to achieve the steady state condition in this experiment. Thus, the experimental and simulation results of stator voltage and the current and phase shift between them at the end of the secondary are shown in Table 3. Of course, according

to the simulation results, the stator current at the steady-state condition is  $i_x = 2.71$  A. As in part 7.1, there is also a good agreement between the simulation and experiment results.

7.3 Locked primary experiment

The effect of the air gap length on the thrust characteristics of the LIM has been discussed in [15]. In order to investigate the air gap length effect on the starting propulsion force, the stator of the experimental model was locked by a mechanical force gauge as shown in Fig. 8. This experiment was carried out for 4 values of the air gap between primary and secondary (air gape= 10 mm, 15 mm, 20 mm and 25 mm).

The thrust versus speed simulated characteristic of the experimental model for these values of air gaps are shown in Fig. 9 and the propulsion thrust versus the air gap length characteristic under locked stator condition ( $S = 1$ ) is shown in Fig. 10. The experimental results from the locked test are presented in Fig. 10. The propulsion forces at unity slip obtained from experiment and simulation are shown in Table 4.

From this experiment, it can be seen that the propulsion force monotonically decreases with air gap length; this phenomenon matches with [15] and [16].

According to these results, the maximum error between the two methods on propulsion force is about 7%. Thus, it is seen that the experimental results are in accordance with the simulation results. Therefore, the experimental and simulation methods have acceptable accuracy.

8 CONCLUSION

In this paper, based on the Duncan’s per-phase equivalent circuit, a dynamic model for short stator LIM with the end effects, which allows fast and accurate simulations, has been developed. The validity of the LIM model and simulation method was checked by comparing the simulation results with the experimental results, obtained from the prototype model.

In this research, in order to validate the simulation results and experimental model, the following experiments have been done:

- Measurement of the equivalent circuit parameters
- Free acceleration experiment
- Locked primary experiment ( $S = 1$ )

Comparing the experimental and simulation results shows that the modelling and simulating procedures and the experimental methods for this type of linear motor have sufficient accuracy. Thus, this model and simulation can be used for design studies, control development, and performance evaluation for a variety of LIM applications. As a final note, the author is still working on modelling and experimental stages in the case of LIMs. In particular, the effects of different parameters of design and different types of power supply, especially PWM inverters, on the

electrical and mechanical specifications of LIMs are being analyzed too.

#### REFERENCES

- [1] HAMZEHB AHM ANI, H.: The Effects of the Voltage Source Inverter Harmonics on Dynamic Performance of Short Rotor Linear Induction Motors, *Word Academy of Science, Engineering and Technology* **62** (Feb 2010), 1256–1263.
- [2] HAMZEHB AHM ANI, H.—SHOULAIE, A.: Investigation of Dynamic Performance of Short Rotor Linear Induction Motor while fed by Different types of Voltage Source Inverters, 16<sup>th</sup> Iranian Conference on Electrical engineering, May 2008, pp. 248–253.
- [3] JUNYONG LU: Dynamic Characteristic Analysis of High Speed Long Primary Block Feeding Linear Induction Motor, *International Conference on Electrical Machines and Systems*, 2008. ICEMS 2008,, 17-20 Oct 2008, pp. 3459–3463.
- [4] GIERAS, J. F.—DAWSON, G. E.—EASTHAM, A. R.: A New Longitudinal end Effect Factor for Linear Induction Motors, *IEEE. Trans.* **EC-22** (1) (1987), 152-159.
- [5] FAIZ, J.—JAFARI, H.: Accurate Modeling of Single-Sided Linear Induction Motor Considers End Effect and Equivalent Thicknesses, *IEEE. Trans.* **MAG-36** (5)— (2000), 3785-3790.
- [6] NONDAHL, T. A.—NOVOTNY, D. W.: Three-Phase Pole-by-Pole Model of a Linear Induction Machine, *IEE Proc. Elect. Power Appl.* **127** (2) (1980), 68-82.
- [7] DUNCAN, J.—ENG, C.: Linear Induction Motor-Equivalent Circuit Model, *IEE Proc., Electr. Power Appl.* **130** (1) (1983), 51-57.
- [8] KANG, G.—NAM, K.: Field-Oriented Control Scheme for Linear Induction Motor with the End Effect, *IEE Proc., Electric Power Application* **152** No. 6 (Nov 2005), 1565-1572.
- [9] CHENG, D. K.: *Field and Wave Electromagnetic*, 2nd edition, Addison Wesley, 1983.
- [10] WEI XU: Equivalent Circuits for Single-Sided Linear Induction Motors, *IEEE Transactions on Industry Applications* **46** No. 6 (Nov/Dec 2010), 2410–2423.
- [11] da SILVA, E. F.—dos SANTOS, E. B.: Dynamic Model for Linear Induction Motors, *IEEE International Conference on Industrial Technology*, vol. 1, 2003, pp. 478-482.
- [12] CHEE-MUN ONG: *Dynamic Simulations of Electric Machinery: Using MATLAB/SIMULINK*, Prentice Hall PTR, 2007.
- [13] IEEE Std 112™–2004 (Revision of IEEE Std 112-1996): *IEEE Standard Test Procedure for Polyphase Induction Motors and Generators*, Nov 2004.
- [14] NASAR, S. A.—BOLDEA, I.: *Linear Electric Motors*, Prentice-Hall, Inc., Englewood Cliffs, New Jersey, 1987.
- [15] NASAR, S. A.—BOLDEA, I.: *Linear Motion Electromagnetic System*, John Wiley & Sons Inc., 1995.
- [16] HAIDONG YU: *High Grade Control of Linear Induction Motor Drives*, PhD thesis, The University of Texas at Arlington in Partial Fulfillment, Texas, USA, December 2007.

Received 11 March 2011

**Hamed HAMZEHB AHM ANI** was born in Sanandaj, Iran in 1978. He received the BSc degree in electrical engineering from Birjand University, Birjand, Iran 2005 and the MSc degree in electrical engineering from Iran University of Science and Technology (IUST), Tehran, Iran 2007. From 2005 to 2008 he was employed as a Supervisor Engineer at Moshanir Power Engineering Consultant, Tehran, Iran. He joined the school of Engineering at Azad university of Sanandaj as an academic staff and researcher. He is currently working towards the PhD degree in electrical engineering at Cardiff University, United Kingdom. His research interests include the design and control of linear electric motors, Power electronics converters and electrical steels.



**EXPORT - IMPORT**  
of periodicals and of non-periodically  
*printed matters, books and CD-ROMs*

Krupinská 4 PO BOX 152, 852 99 Bratislava 5, Slovakia  
tel: ++421 2 638 39 472-3, fax: ++421 2 63 839 485  
[info@slovart-gtg.sk](mailto:info@slovart-gtg.sk); <http://www.slovart-gtg.sk>

